Supporting information for

A Designed Second-Sphere Hydrogen-bond Interaction That Critically Influences The O-O Bond Activation for Heterolytic Cleavage in Ferric Iron-Porphyrin Complexes

Sarmistha Bhunia[1], Atanu Rana[1], Somdatta Ghosh Dey[1,], Anabella Ivancich[2*], Abhishek Dey[1*]*

[1]Department of Inorganic Chemistry, Indian Association for the Cultivation of science, Kolkata, India, 700032

[2]CNRS, Aix-Marseille Univ, Laboratoire de Bioénergétique et Ingénierie des Protéines (UMR 7281), IMM FR3479, Marseille, France.

Table of Contents

1. Stopped-flow kinetics and absorption spectroscopy

1.a. Figure S1

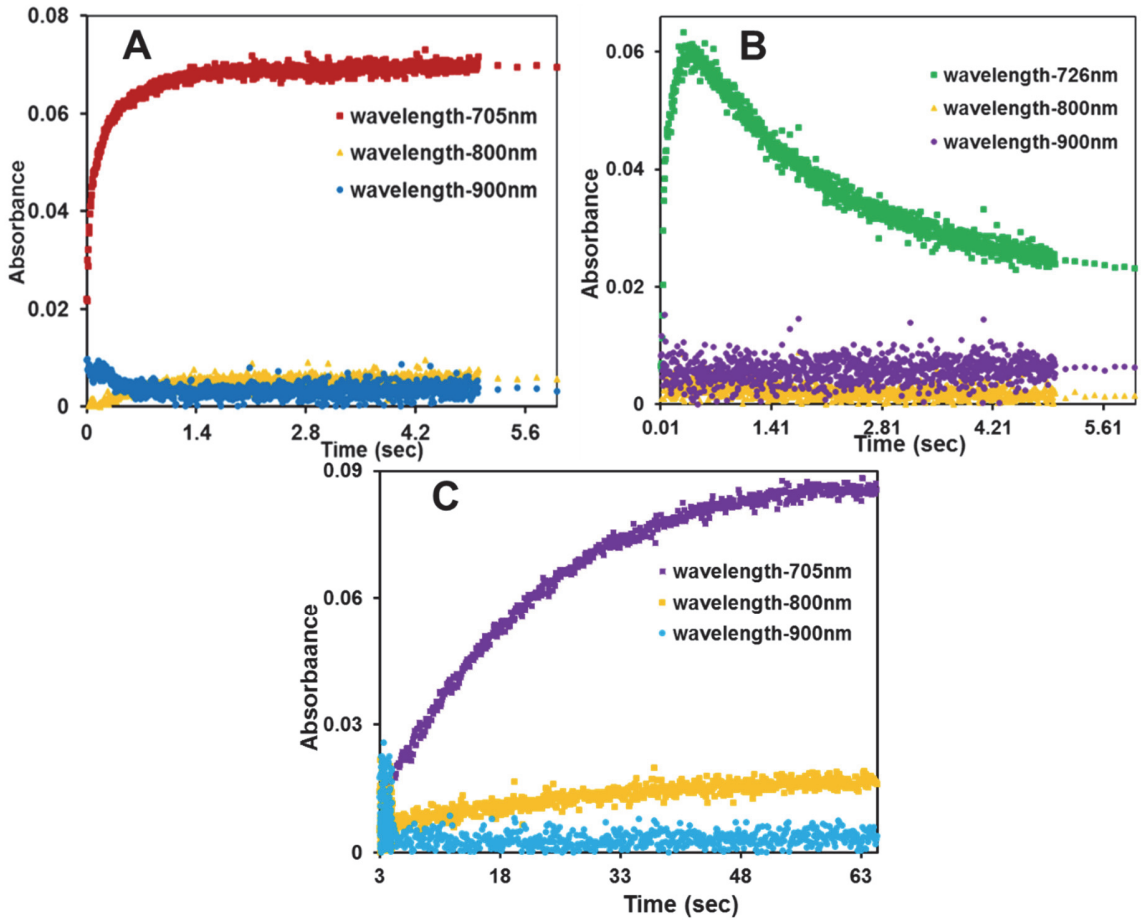

Figure S1. Time traces for kinetics of A) 705 nm (Compound I), 800 nm and 900 nm bands (isoporphyrin intermediate) of Fe^{III}L2(Br); B) 726 nm (Compound I), 800 nm and 900 nm bands of Fe^{III}L3(Br) at 6sec and C) 705 nm (Compound I), 800 nm and 900 nm bands of Fe^{III}MPh(Br).

1.b. Figure S2 and Scheme S1

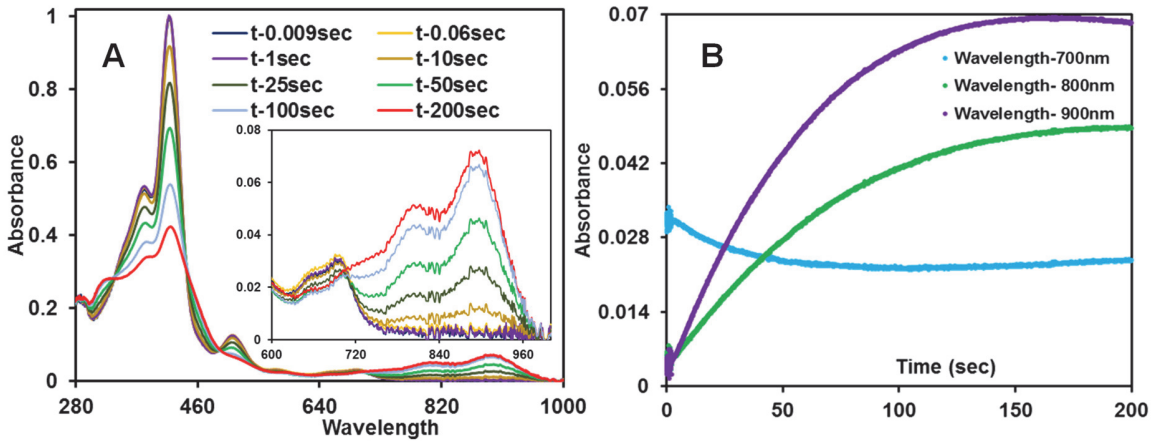

Figure S2. Absorption spectral changes of $Fe^{III}TPP$ (50 µM) after addition of 4eq mCPBA (200 µM) in dichloromethane at -30ºC using stopped flow spectro-photometer. Panel A) resting $Fe^{III}TPP(Br)$ at the beginning of the reaction (blue trace), intermediate within 200 sec (red trace) corresponding to isoporphyrin species. Time evolution of intermediate species are also shown. Panel B) Time traces for the decay of charge transfer band at 700nm, rise of 800nm and 900nm bands.

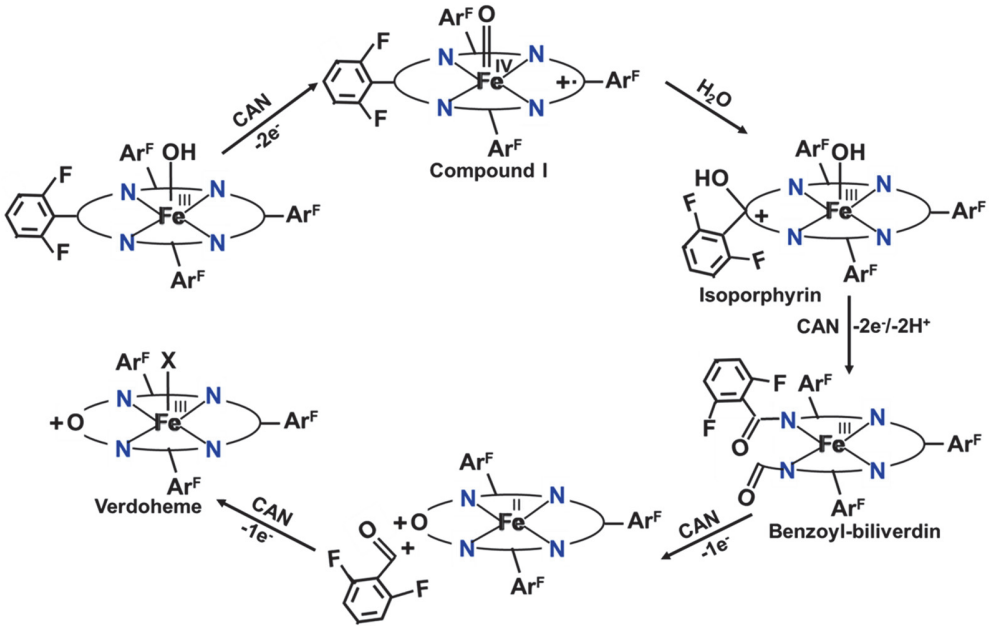

Scheme S1. Proposed mechanism for the oxidation of a Fe(III)-OH complex analogous to $Fe^{III}TPP(Br)$ to verdoheme via isoporphyrin.

1.c. Figure S3

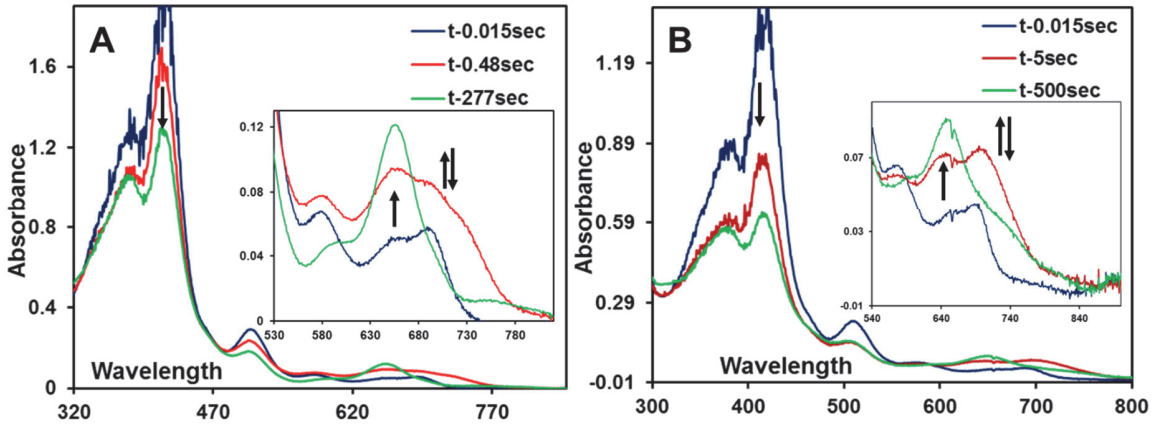

Figure S3. Stopped flow absorption spectral change after the reaction of A) $Fe^{III}L3(Br)$ and B) $Fe^{III}L2(Br)$ with mCPBA in dichloromethane at -30ºC. In (A) blue solid line: resting $Fe^{III}L3$ at the beginning of the reaction, Red line: the intermediate formed at 500msec corresponding to $[Fe^{IV}=O\ Por^{\bullet+}]L3$, Green line: the formation of another intermediate corresponding to Compound II, $(Fe^{IV}=O)L3$ at 277sec ; In (B) Blue line : resting $Fe^{III}L2$ at the beginning of the reaction, Red line : the intermediate formed at 5sec corresponding to $[Fe^{IV}=O\ Por^{\bullet+}]L2$. Green line: the formation of another intermediate corresponding to Compound II, $(Fe^{IV}=O)L2$ at 500sec.

1.d. Figure S4

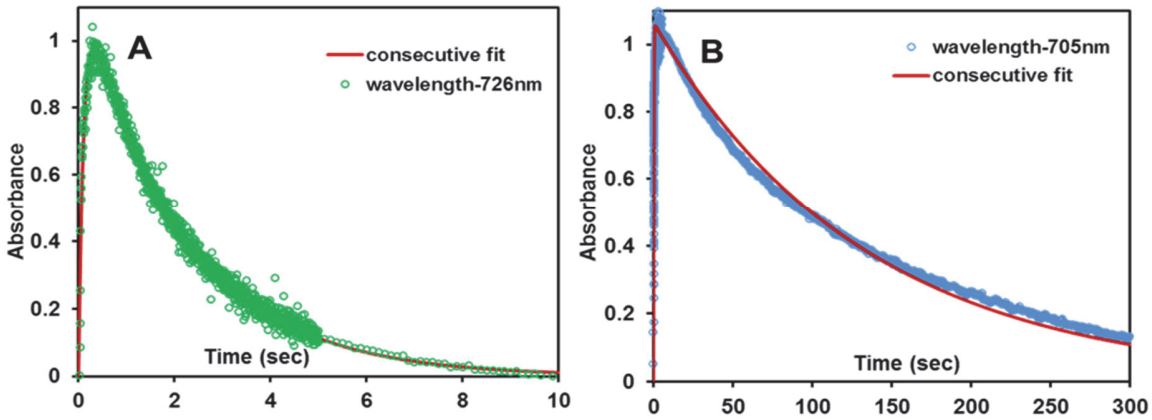

Figure S4. Consecutive fits for the formation and decay of Compound I at 726 nm and 705 nm for A) $Fe^{III}L3(Br)$ and B) $Fe^{III}L2(Br)$ respectively.

1.e. Calculation of $\Delta G^{\#}$ based on the temperature dependent kinetics of Compound I formation

We have examined temperature dependent kinetics for Compound I formation of $Fe^{III}L2(Br)$ with mCPBA in dichloromethane. From the Eyring equation, we have determined the $\Delta H^{\#}$ and $\Delta S^{\#}$ separately varying temperature from 240 K to 260 K and then calculated the $\Delta G^{\#}$ using the equations given below.

$$\ln (k/T) = -\Delta H^{\#}/RT + \ln(k'/h) + \Delta S^{\#}/R \quad \ldots\ldots(1)$$

$$\text{and } \Delta G^{\#} = \Delta H^{\#} - T\Delta S^{\#} \quad \ldots\ldots(2)$$

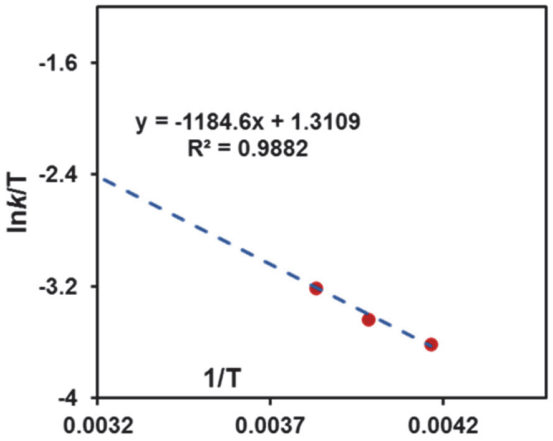

From equation (1), $\Delta H^{\#}$ and $\Delta S^{\#}$ can be derived from the slope and intercept of the ln(*k*/T) vs 1/T plot.

Hence, $\Delta H^{\#}/R = 1184.6$ and $\ln(k'/h) + \Delta S^{\#}/R = 1.31$

Putting the values of other constant terms,

we have, $\Delta H^{\#} = 2.34 \pm 0.2$ kcal/mol and $\Delta S^{\#} = -44.60 \pm 1$ cal mol^{-1} K^{-1}

From equation (2), Gibbs free energy of activation $\Delta G^{\#} = 13.03 \pm 0.2$ kcal/mol

1.f. The g ≈ 6 spectral region of the 9-GHz EPR spectra for the Fe^{III}L3 porphyrin complex in dichloromethane in the resting ferric state and upon reaction with *m*-chloroperbenzoic acid.

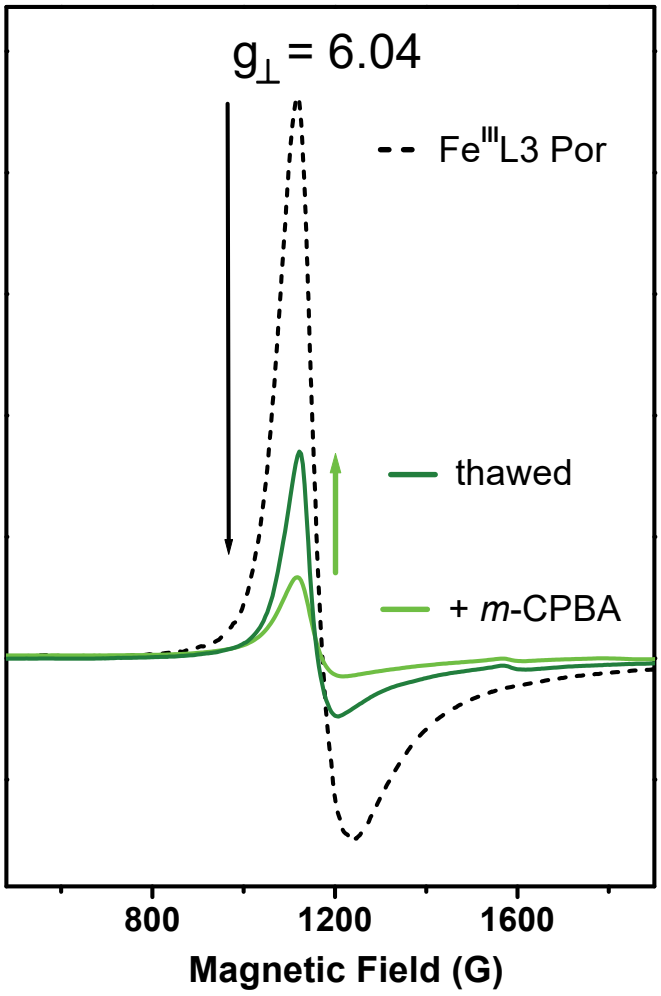

Figure S5. The 9-GHz EPR spectra (g ≈ 6 spectral region) of the Fe^{III}L3 porphyrin complex in dichloromethane for the resting ferric state (dotted black trace) and after reaction with *m*-chloroperbenzoic acid (light green trace). The reaction was done in a cold bath (*ca.* -100°C) and using a mixing time of 3s, before freezing the sample in liquid nitrogen. The experimental conditions (concentrations and instrument parameters) are the same as in Fig. 7.

The clear decrease in intensity (85%, black arrow) of the $g_{\perp}$= 6.04 component of the heme iron (axial) spectrum upon reaction with *m*-CPBA reflects the change in oxidation state of the heme iron, i.e. formation of the high-valent intermediate(s). Accordingly, a new and distinct EPR

signal of the [Fe^{IV}=O $Por^{\bullet+}$] intermediate with $g_{\perp}^{eff}$ = 3.80 and $g_{\parallel}^{eff}$ = 1.99 was observed (see Fig. S6, Panel B light green trace). Thawing the same sample to 20°C during 20 min resulted in the complete disappearance of the [Fe^{IV}=O $Por^{\bullet+}$] intermediate (see Fig. S6, Panel B brown trace) and a concomitant increase (55%) of the ferric EPR signal (dark green trace).

1.g. The 9-GHz EPR spectra, recorded at 4K, of the Fe^{III}L3 porphyrin complex showing the step-by-step changes upon reaction with *m*-chloroperbenzoic acid as oxidant, and as a function of oxidant excess and mixing time/temperatures.

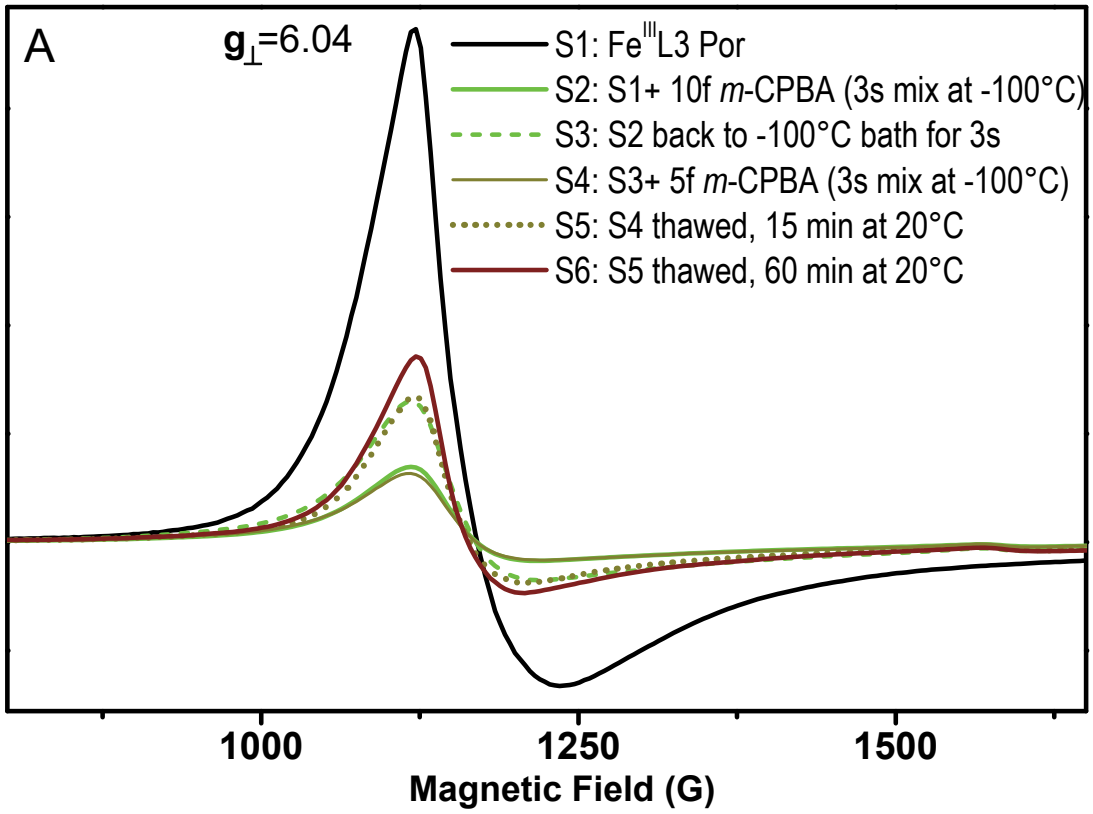

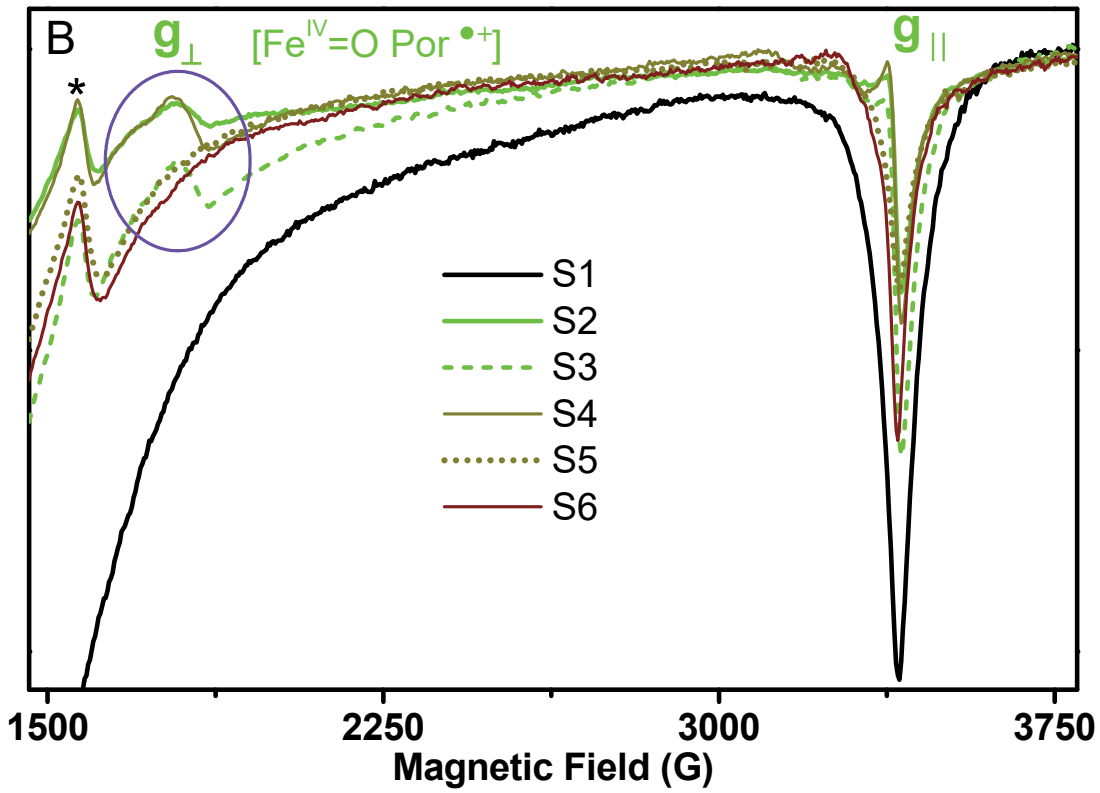

Figure S6. The 9-GHz EPR spectra, recorded at 4K, of the Fe^{III}L3 porphyrin complex showing the step-by-step changes upon reaction with *m*-chloroperbenzoic acid (*m*-CPBA) and as a function of oxidant excess and mixing time/temperatures. The same EPR sample (s1), kept in the same EPR tube, was exposed to sequential treatments labelled s2 to s6. Two spectral regions of the EPR spectrum ($g \approx 6$, Panel A and $4.5 > g > 1.85$, Panel B) are shown separately for clarity. The experimental conditions (concentrations and instrument parameters) are the same as in Fig. 7.

s1 (black dotted trace): Fe^{III}L3 porphyrin complex in DCM

s2 (light-green trace): 10-fold molar excess (final concentration) of *m*-CPBA in DCM was added, directly in the EPR tube immersed in a cold bath (ca. -100 °C), to **s1**. After mixing during 3s, the sample was frozen in liquid nitrogen. (Panel A) The decrease of the ferric EPR signal (85%) shows the change in oxidation state of the ferric iron to the high-valent intermediate(s).

(Panel B) The concomitant appearance of the EPR signal of an exchange-coupled oxoferryl-porphyrin radical species, [Fe^{IV}=O $Por^{\bullet+}$] (Compound I) with $g_{\perp}^{eff} = 3.80$ and $g_{\parallel}^{eff} = 1.99$. The contribution of an EPR silent species, [Fe^{IV}=O] (Compound II) is concluded to account for the decrease of the initial ferric signal.

s3 (dotted light-green trace): s2 was put back in the cold bath (-100 °C) during 3s, then frozen again in liquid nitrogen. The increase of the ferric EPR signal (55% increase as compared to s2 ferric signal)

and no significant change in the [Fe^{IV}=O $Por^{\bullet+}$] EPR signal, that can be rationalized by the reaction of the [Fe^{IV}=O] intermediate with remaining *m*-CPBA, as in the case of chloroperoxidase.[66]

s4 (dark-yellow trace): s3 was quickly thawed (*in an ice bucket*) then, back in the -100 °C bath, 5fold (molar) excess of *m*-CPBA was added and mixed during 3s, before freezing back in LN2. The very same overall EPR spectrum of sample s2, with the same yield of Compound I signal (Panel B) and the same conversion of the ferric signal (Panel A) was observed, indicating that it is possible to cycle back the Fe^{III}L3 porphyrin complex.

s5 (dotted dark-yellow trace): s4 was thawed to *room temperature* and incubated during 15 at 20 °C, then frozen again in liquid nitrogen. The total disappearance of the [Fe^{IV}=O $Por^{\bullet+}$] species (Panel B), expected due to the short-lived character of the intermediate, and a partial recovery (55% as compared to s4) of the ferric signal. The later could be rationalize by the reaction of the [Fe^{IV}=O] intermediate with remaining *m*-CPBA as substrate.

s6 (brown trace): s5 was thawed to room temperature and incubated during 60 min at 20 °C, then frozen again in liquid nitrogen. Further recovery of the ferric EPR signal due to the slow conversion of the [Fe^{IV}=O] intermediate back to ferric (reaction of Compound II with remaining *m*-CPBA).

1.h. Figure S7

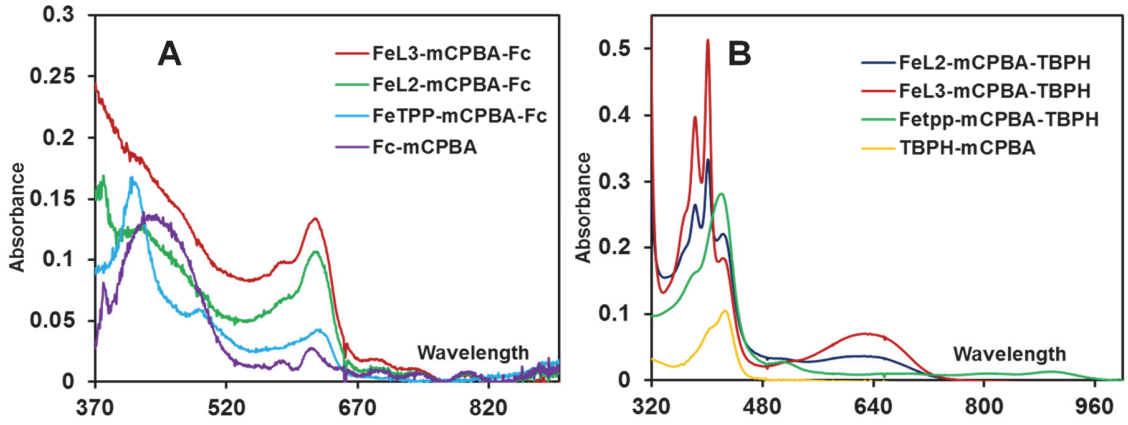

Figure S7. The UV-vis electronic absorption spectra of Fe^{III}L2(Br), Fe^{III}L3(Br), Fe^{III}TPP(Br) complexes as catalyst and ferrocene/TBPH as substrates with mCPBA as oxidant using dichloromethane solvent at room temperature for A) formation of ferrocenium at 620 nm by the addition of iron-porphyrins (4μM) with mCPBA (250 eq, 1mM) and ferrocene (500 eq, 2mM); B) formation of 2,4,6-tri tertiary butyl phenoxyl radical due to oxidation of TBPH with characteristic absorption features at 380nm, 400 nm and 625 nm by adding iron porphyrins (4μM) with mCPBA (250 eq, 1mM) and TBPH (500eq , 2mM).

1.i. Figure S8

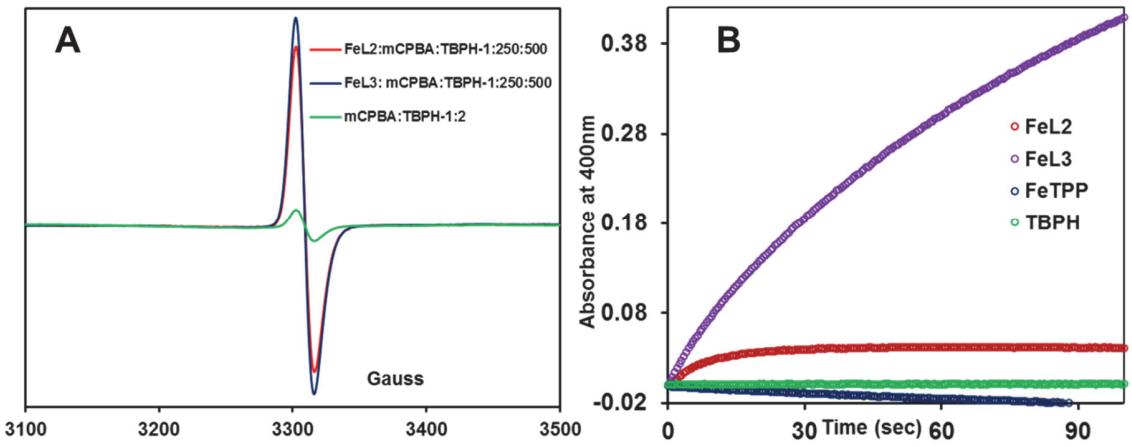

Figure S8. Panel A: 77K 9-GHz EPR spectra of 2,4,6-tri tertiarybutyl phenoxy radical (g≈2) formed upon reaction of (2mM) TBPH with (1mM) mCPBA as oxidant, with no catalyst (green trace), and in the presence of 4μM Fe^{III}L2 (red trace) and 4μM Fe^{III}L3 (blue trace). Experimental condition: temperature = 77 K, microwave frequency = 9.118 GHz, microwave power = 2 mW, modulation amplitude = 40 kHz, modulation width = 1 mT, time constant = 0.03). Pane B: Time traces for formation of 2,4,6-tri tertiary butyl phenoxyl radical due to oxidation of TBPH at 400 nm by adding iron porphyrins (4 μM) with mCPBA (250 eq, 1 mM) and TBPH (500 eq, 2 mM).

1.j. Figure S9

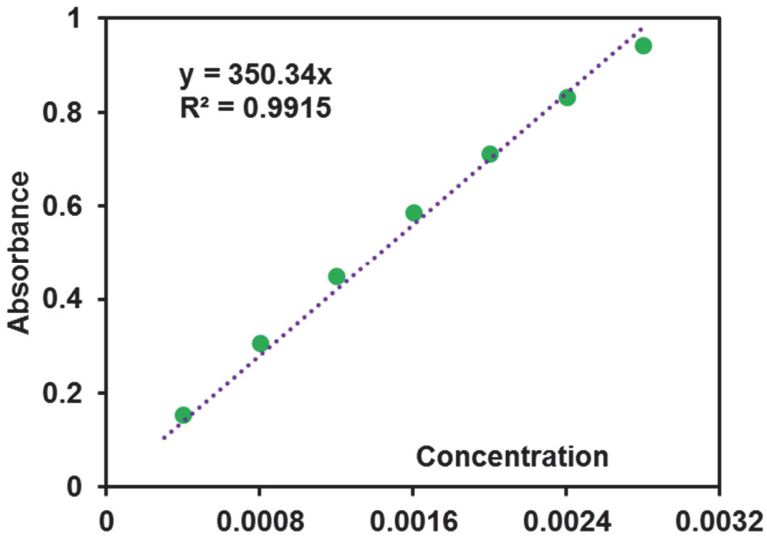

Figure S9. Absorbance vs Concentration plot for ferrocenium hexafluoro phosphate. The molar extinction co-efficient (ε) have been determined using the equation of "Lambert-Beer" law A= ε*c*l ; here the path length of the cuvette l= 1 cm. For ferrocenium hexafluorophosphate, ε value obtained from the slope of the linear plot is 350.34 $M^{-1}cm^{-1}$.

1.k. Figure S10

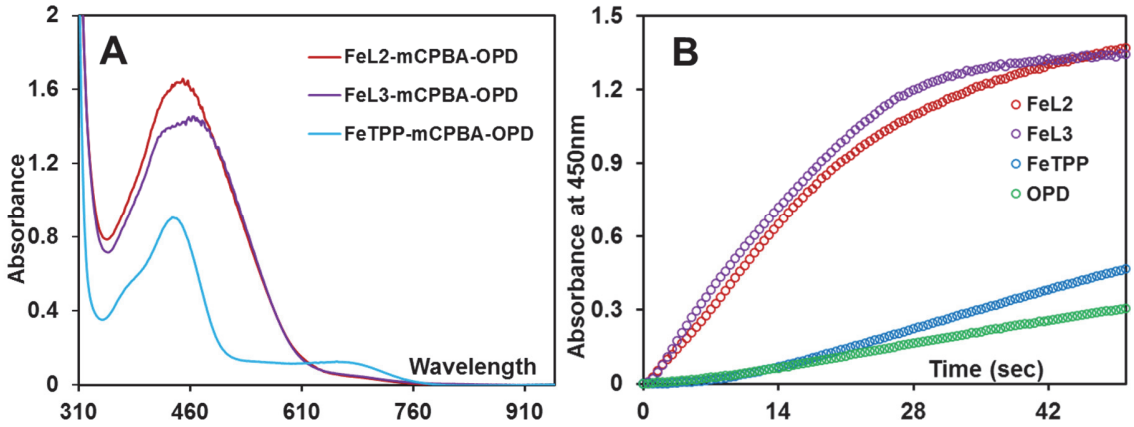

Figure S10. The UV-vis electronic absorption spectra of $Fe^{III}L2(Br)$, $Fe^{III}L3(Br)$, $Fe^{III}TPP(Br)$ complexes as catalyst and o-phenylene diamine (OPD) as substrate with *m*-CPBA (oxidant) for A) Absorbance due to the formation of oxidised product 2,3-diaminophenazine with characteristic absorption feature at a wavelength of 450 nm (red trace:

Fe^{III}L2, violet trace: Fe^{III}L3 and sky blue trace: Fe^{III}TPP) ; B) Time traces for the oxidation of OPD at 450nm by the addition of iron-porphyrins (4μM) with mCPBA (250eq, 1mM) and OPD (500eq, 2mM).

2. DFT optimised structures

2.a. Figure S11

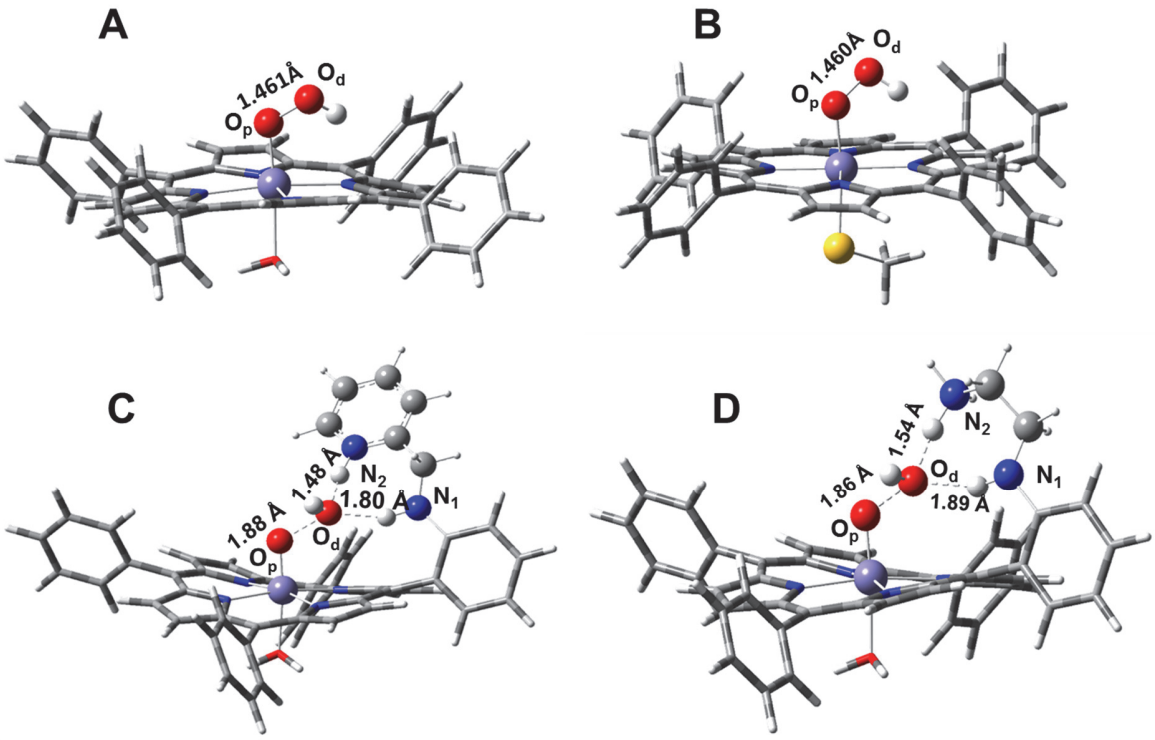

Figure S11. Optimized structures of six coordinate low spin (A) [Fe^{III}TPP-OOH]; (B) [Fe^{III}TPP-(S-Me)OOH]; (C) [Fe^{III}L2-OOH]H^+; (D) [Fe^{III}L3-OOH]H^+ with hydroperoxide and water as axial ligands and protonated distal amines in PCM model considering dichloromethane as solvent. *color codes*: carbon → *grey*, hydrogen→ white, nitrogen → *blue*, oxygen → *red*, and iron → *bluish grey.*

2.b. Figure S12

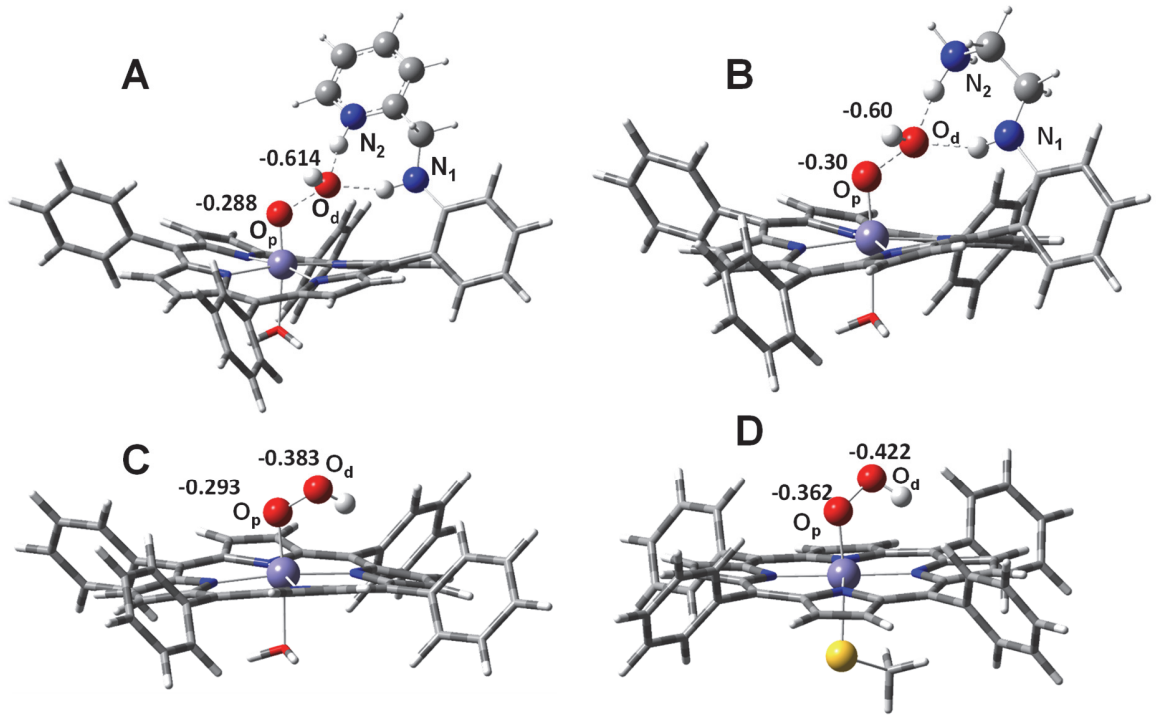

Figure S12. Optimized structures of (A) $[Fe^{III}L2\text{-}OOH]H^{+}$; (B) $[Fe^{III}L3\text{-}OOH]H^{+}$; (C) $[Fe^{III}$-TPP-OOH] and (D) $[Fe^{III}$TPP-SMe-OOH] with hydroperoxide and water as axial ligands with the mulliken charges on proximal and distal oxygen atoms. *color codes*: carbon → *grey*, hydrogen→ white, nitrogen → *blue*, oxygen → *red*, sulphur → *yellow*, and iron → *bluish grey.*

3. MO diagram

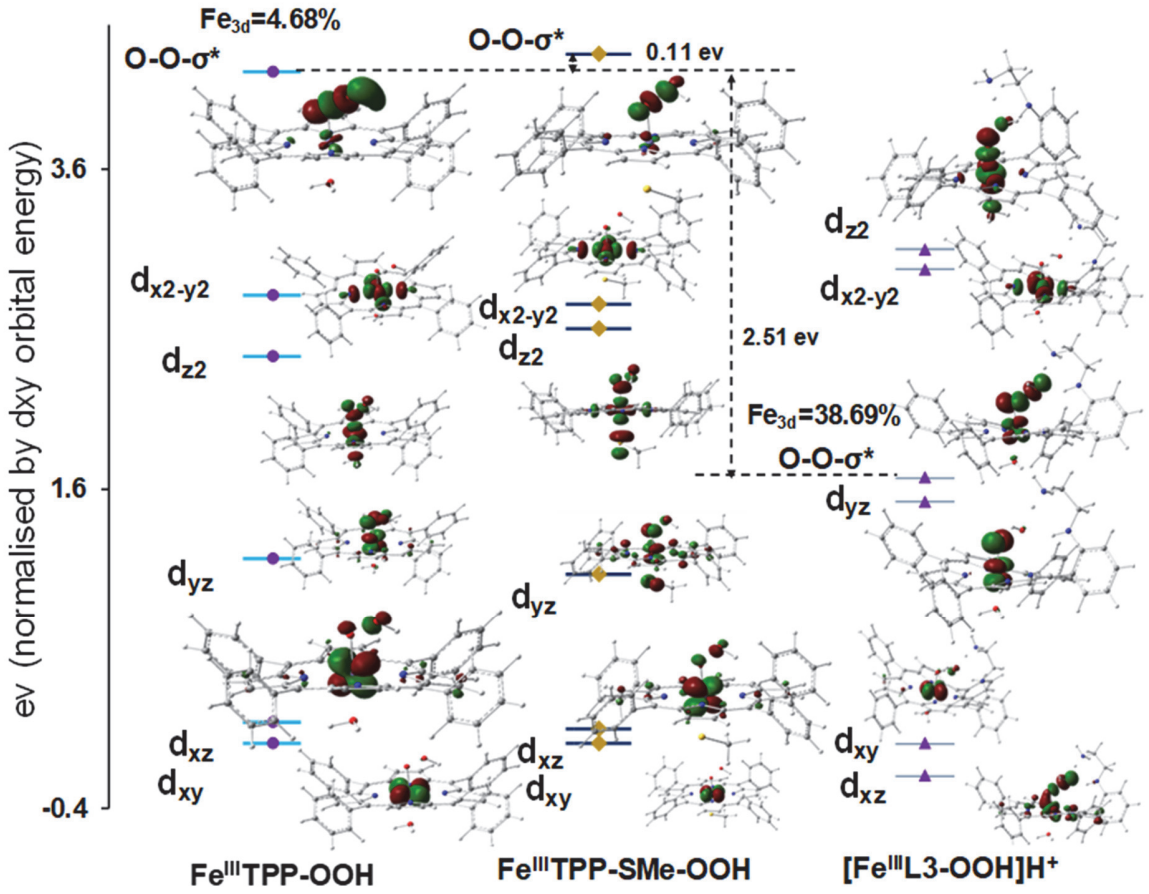

Figure S13. Calculated (BP86) GS MO diagram of Fe(III)TPP-OOH (no axial thiolate), [Fe(III)-TPP-SMe-OOH] (axial thiolate ligand), [Fe(III)L3-OOH]H+ (protonated H-bonding residue). Only β orbital are shown. The relative energies are normalized with respect to the non-bonding dxy orbital. The occupied dxz orbital interacting with unoccupied O-O σ* orbital for the protonated second sphere residues but no such interaction is present in FeTPP-SCH3-OOH.

4. Orbital Contributions

Table S1 : Orbital contributions(%) of associated atoms of Fe^{III}-TPP-OOH

FeTpp	Fe	$4N_{pyr}$	$Fe+4N_{pyr}$	O_p	O_d	O_{total}
d_{xy}	87.48	0.75	88.23	0.12	0.37	0.49
d_{xz}	71.16	2.19	73.35	0.94	2.68	3.62
d_{yz}	53.34	0.9	54.24	13.15	2.79	15.94
d_{z2}	62	4.32	66.32	9.69	2.95	12.64
d_{x2-y2}	67.93	15.42	83.35	0.31	0.15	0.46
O-Oσ*	3.99	0.87	4.86	22.55	16.87	39.42

Table S2 : Orbital contributions(%) of associated atoms of Fe^{III}-TPP-SMe-OOH

FeTpp-SMe-OOH	Fe	$4N_{pyr}$	$Fe+4N_{pyr}$	O_p	O_d	O_{total}	S
d_{xy}	88.7	0.47	89.17	0.16	0.16	0.32	1.5
d_{xz}	68.73	0.84	69.57	1.03	1.85	2.88	1.47
d_{yz}	65.96	8.01	73.97	11.19	2.43	13.62	13.56
d_{z2}	57.07	4.98	62.05	7.86	2.75	10.61	16.24
d_{x2-y2}	66.86	14.04	80.9	0.38	0.19	0.57	0.63
O-Oσ*	2.03	1.76	3.79	7.45	5.2	12.65	7.34

Table S3: Orbital contributions(%) of associated atoms of $[Fe^{III}$-L2-OOH$]H^{+}$

$[FeL2\text{-}OOH]H^{+}$	Fe	$4N_{pyr}$	$Fe+4N_{pyr}$	O_p	O_d	O_{total}
d_{xz}	26.58	10.49	37.07	4.41	13.14	17.55
d_{xy}	75.47	1.46	76.93	0.27	1.14	1.41
d_{yz}	59.48	1.64	61.12	18.12	0.53	18.65
d_{x2-y2}	63.62	18.43	82.05	0.09	0.01	0.1
d_{z2}	52.05	6.28	58.33	14.41	1.74	16.15
O-Oσ*	37.04	1.65	38.69	25.25	11.58	36.83

5. Synthesis and Characterisation

5.a.

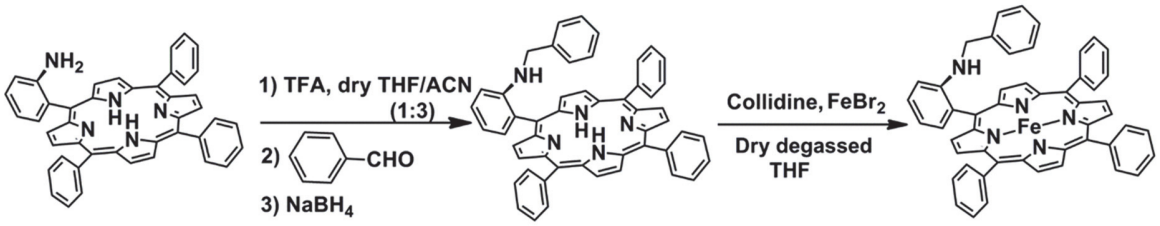

Scheme S2. Synthesis of FeMPh.

5.b. Absorption spectra

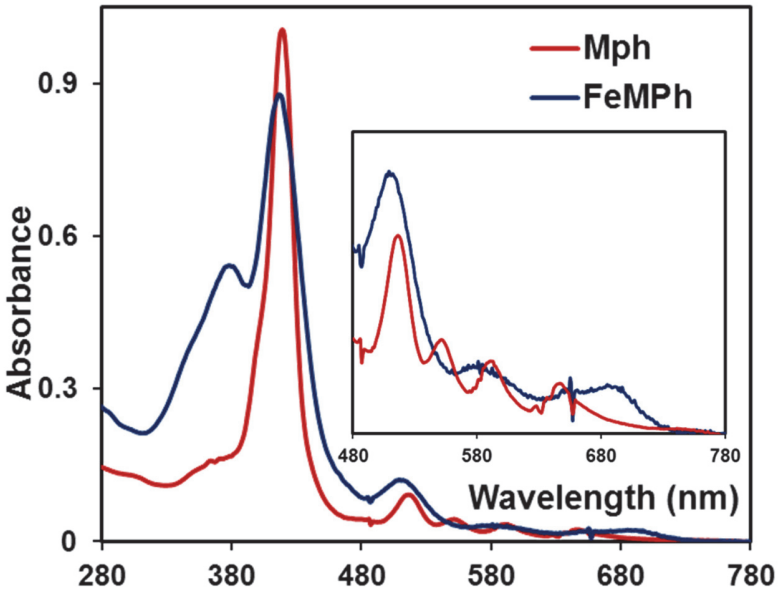

5.c. ESI-MS spectra of Mph

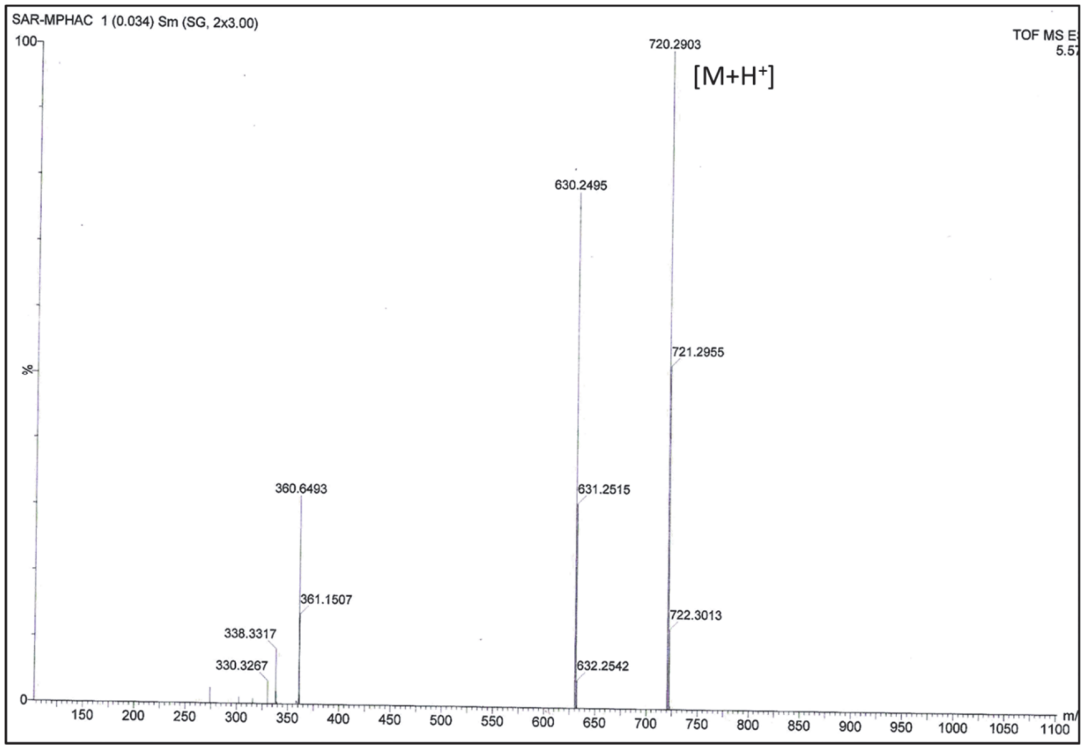

5.d. ^{1}H-NMR spectra of MPh

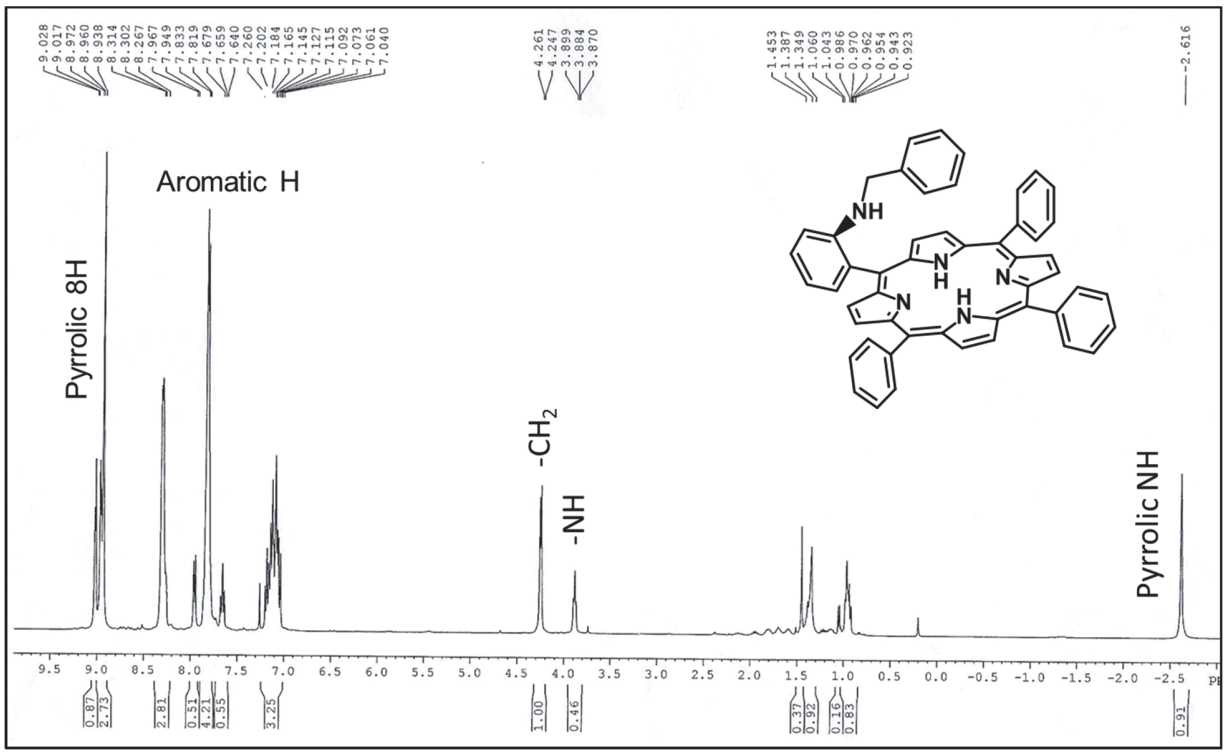

5.e. ESI-MS spectra of FeMPh

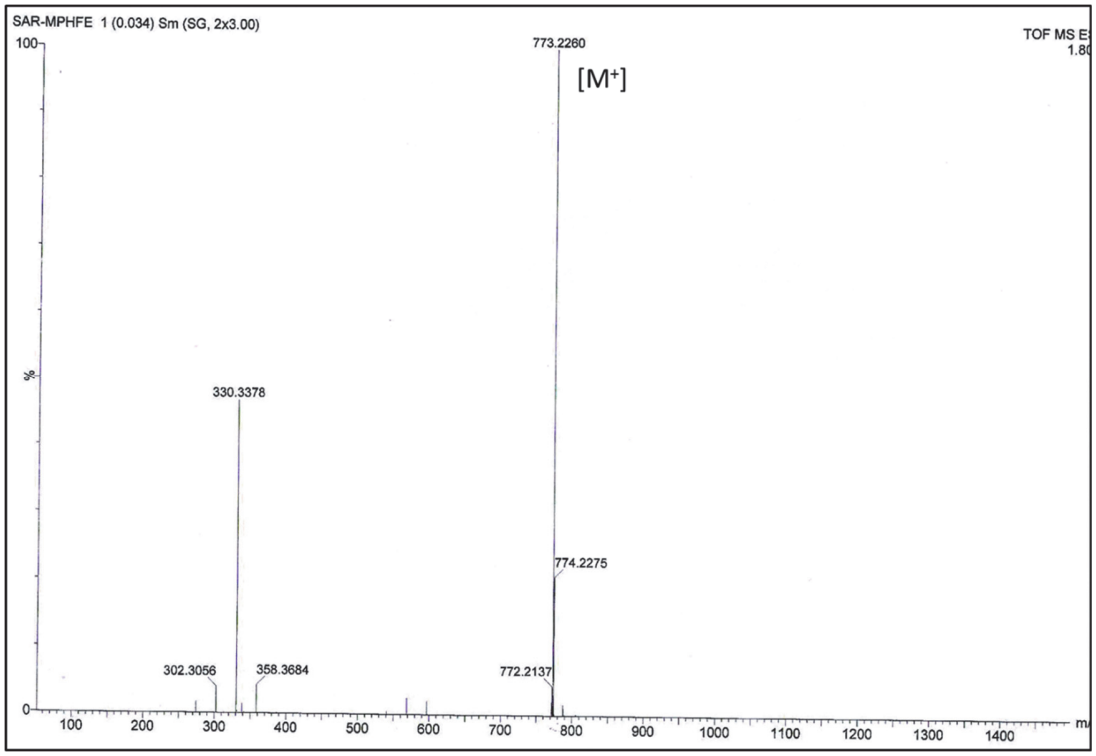

5.f. ^{1}H-NMR spectra of FeMPh

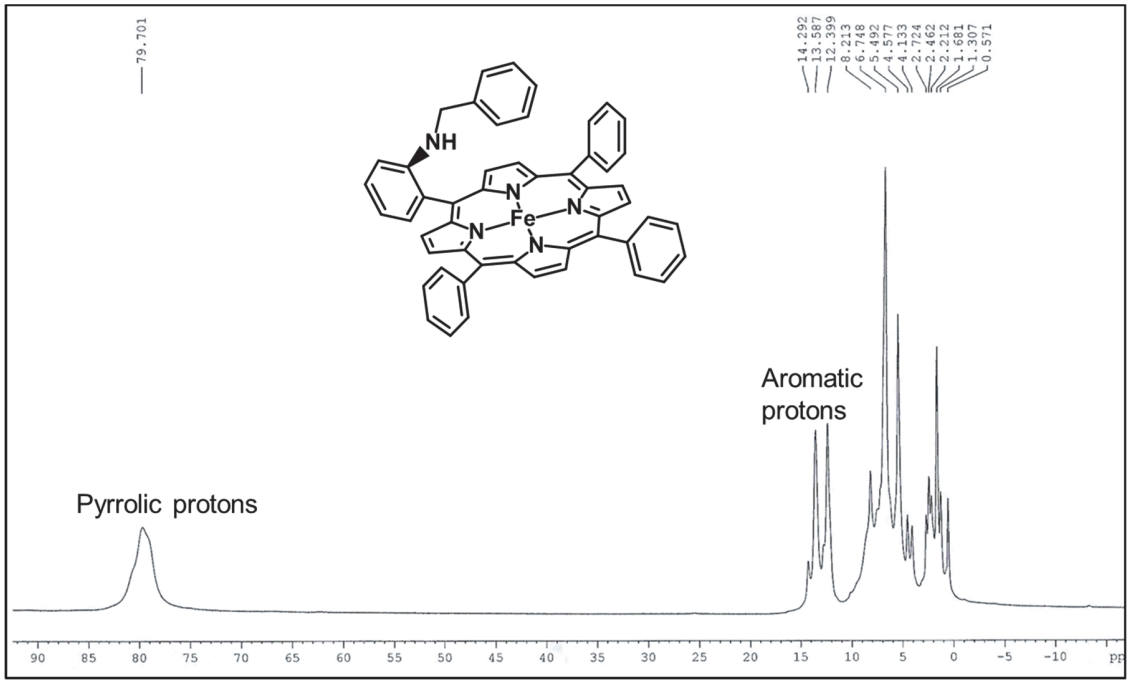
79.701
14.292
13.587
12.399
8.213
6.748
5.492
4.577
4.133
2.724
2.462
2.212
1.681
1.307
0.571
NH
N
Fe
N
N
N
Aromatic protons
Pyrrolic protons
90 85 80 75 70 65 60 55 50 45 40 35 30 25 20 15 10 5 0 -5 -10